Weibel instability and structures of magnetic island in anti-parallel collisionless magnetic reconnection

San Lu,[1,2] Quanming Lu,[1,a)] Xi Shao,[3] Peter H. Yoon,[4,5] and Shui Wang[1]
[1]*CAS Key Laboratory of Basic Plasma Physics, Department of Geophysics and Planetary Sciences, University of Science and Technology of China, Hefei, 230026, China*
[2]*State Key Laboratory of Space Weather, Chinese Academy of Sciences, Beijing 100190, China*
[3]*Department of Astronomy, University of Maryland, College Park, Maryland 20742, USA*
[4]*Institute for Physical Science and Technology, University of Maryland, College Park, Maryland 20742, USA*
[5]*School of Space Research, Kyung Hee University, 446-701, Korea*

(Received 31 March 2011; accepted 2 June 2011; published online 14 July 2011)

Two-dimensional (2D) particle-in-cell simulations are performed to investigate the structures of the out-of-plane magnetic field in magnetic island, which is produced during anti-parallel collisionless magnetic reconnection. Regular structures with alternate positive and negative values of the out-of-plane magnetic field along the x direction are formed in magnetic island. The generation mechanism of such structures is also proposed in this paper, which is due to the Weibel instability excited by the temperature anisotropy in magnetic island. © *2011 American Institute of Physics*. [doi:10.1063/1.3605029]

I. INTRODUCTION

Magnetic reconnection is a fundamental plasma process, which is widely accepted to be the major driving mechanism for many explosive phenomena in space and laboratory plasmas. During magnetic reconnection, magnetic energy is rapidly converted into plasma kinetic energy, which is accompanied by topological changes of magnetic field lines.[1–3] Energetic electrons are considered to be an important signature in magnetic reconnection.[4–6] In solar flares, x ray is thought to be generated by energetic electrons in magnetic reconnection,[8–10] and there are direct measurements of energetic electrons up to several hundreds of keV associated with magnetotail reconnection.[11–16]

Electron behaviors in magnetic reconnection with a single X-line have been thoroughly studied with self-consistent particle-in-cell simulatons.[17–19] In anti-parallel reconnection, electrons firstly move toward the X-line along the separatrices because of the magnetic mirror effects,[19] and then they are accelerated in the vicinity of the X-line and the pileup regions by the reconnection electric field. Most of the electrons accelerated in the vicinity of the X-line come from the regions just outside of the separatrices, while most of the electrons accelerated in the pileup regions come from the regions inside of the separatrices.[20] In guide field reconnection, electrons can be accelerated by the parallel electric field in the vicinity of the X-line, as well as when they move toward the X-line.[4,20]

When there are two X-lines developed simultaneously in a current sheet, a magnetic island will be formed between the two X-lines. Magnetic island with bipolar signature in the north-south magnetic field component B_z have been directly observed in the magnetotail, and there are also observational evidences showing the enhancement of energetic electron fluxes inside magnetic island.[13,15,16,21] The resultant energetic electrons are predicted theoretically to have a power-law spectrum with a spectral index consistent with the observations in the magnetotail.[11,22,23] Obviously, the structures of magnetic island have great influences on electron behaviors. In this paper, two-dimensional (2D) particle-in-cell (PIC) simulations are performed to investigate the structures of magnetic island formed in anti-parallel multiple X line reconnection. Regular structures with alternate positive and negative values of the out-of-plane magnetic field are formed in magnetic island, and their generation mechanism is also discussed.

The paper is organized as follows. In Sec. II, we describe our 2-D PIC simulation model. In Sec. III, the simulation results are presented. The conclusions and discussion are given in Sec. IV.

II. SIMULATION MODEL

2D PIC simulations are employed in this paper. In the simulations, the electromagnetic fields are defined on the grids and updated by solving the Maxwell equations with a full explicit algorithm. The ions and electrons are advanced in the electromagnetic fields. The initial equilibrium configuration is chosen to use a one-dimensional (1D) Harris current sheet geometry in the (x, z) plane, where the magnetic field and density can be described as

$$\mathbf{B}_0(z) = B_0 \tanh(z/\delta)\mathbf{e}_x \tag{1}$$

$$n(z) = n_b + n_0 \sec \mathrm{h}^2(z/\delta) \tag{2}$$

where B_0 is the asymptotical magnitude of the magnetic field, δ is the half width of the current sheet, n_b is the density of the background plasma, and n_0 represents the peak Harris density. Initially, a Maxwellian distribution is adopted in the simulations for each species of particles (ions and electrons). The initial ion distribution is isotropic with temperature T_{i0}. Both isotropic and anisotropic electron distributions are used

a)Author to whom correspondence should be addressed. Electronic mail: qmlu@ustc.edu.cn.

in this paper. We assume that $T_{\perp e0}$ and $T_{||e0}$ represent the initial electron temperatures perpendicular and parallel to the magnetic field, respectively. The drift speeds of ions and electrons in the y direction satisfy the equation $V_{i0}/ = -T_{i0}/T_{\perp e0}.V_{e0} = -T_{i0}/T_{\perp e0}$,[24] where V_{i0} (V_{e0}) are the drift speed of ions(electrons). We set $T_{i0}/T_{e\perp 0} = 4$, and $n_b = 0.2n_0$. The mass ratio of the ion to electron is chosen to be $m_i/m_e = 100$. The light speed is $c = 15v_A$, where v_A is the Alfven speed based on B_0 and n_0.

The computation is carried out in a rectangular domain in the (x, z) plane. The spatial resolution is $\Delta x = \Delta z = 0.05c/\omega_{pi} = 0.5c/\omega_{pe}$, where c/ω_{pi} (c/ω_{pe}) is the ion(electron) inertial length, which is based on n_0. The grid number is $N_x \times N_z = 512 \times 128$. Therefore, the size of the computation domain is $L_x \times L_z = (25.6c/\omega_{pi}) \times (6.4c/\omega_{pi})$. The time step is $\Omega_i \Delta t = 0.001$, where $\Omega_i = eB_0/m_i$ is the ion gyrofrequency. In the simulations, there are average about one hundred pairs of ions and electrons in every cell to represent the plasma for the Harris current sheet, and the same number of particles is also employed to represent the background plasma. The periodic boundary conditions are used along the x direction, so the particles which leave the simulation domain from one side will enter again from the other side. At the same time, ideal conducting boundary conditions for the electromagnetic fields and reflected boundary conditions for particles are used along the z direction.

III. SIMULATION RESULTS

Three runs are performed in this paper. In the first run, the half width of the current sheet is $\delta = 0.5c/\omega_{pi}$, the initial electron distribution is isotropic. For the purpose of making the system go into the nonlinear stage and form magnetic island more quickly, an initial flux perturbation is added to modify the Harris current sheet configuration, which can be expressed as

$$\psi(x, z) = -\psi_0 \cos[4\pi(x - L_x/2)/L_x] \cos[\pi z/L_z] \qquad (3)$$

where ψ is the vector potential component A_y, and the perturbation amplitude is $\psi_0/(B_0 c/\omega_{pi}) = 0.05$.

In the second and third runs, the initial electron distribution is assumed to be anisotropic with $A_{e0} = T_{||e0}/T_{\perp e0} - 1 = 0.8$. The half widths of the current sheet is $\delta = 2.0c/\omega_{pi}$ and $\delta = 0.5c/\omega_{pi}$ for Run 2 and Run 3, respectively. No initial flux perturbation is added in both the second and third runs. The tearing mode is stable in Run 2 and Run 3 according to the linear stable condition.[25]

Figure 1 shows the out-of-plane magnetic field B_y/B_0 at $\Omega_i t$ =2.5, 10.5, 17.5, 21.5, and 32 for Run 1, and the magnetic field lines in the (x, z) plane are also plotted. At about $\Omega_i t$ =10.5, two X-lines are formed in the simulation domain, and there are two magnetic islands between them. The out-of-plane magnetic field B_y exhibits characteristic quadrupole structures around the X-lines, which are generated by the current systems in the (x, z) plane. Such in-plane current systems are considered to be formed by the flowing electrons toward the X-lines along the separatrices and the electrons directed away from the X-lines along the magnetic field lines just inside the separatrices after they are accelerated in the vicinity of the X-lines.[19] As time goes on, the amplitude

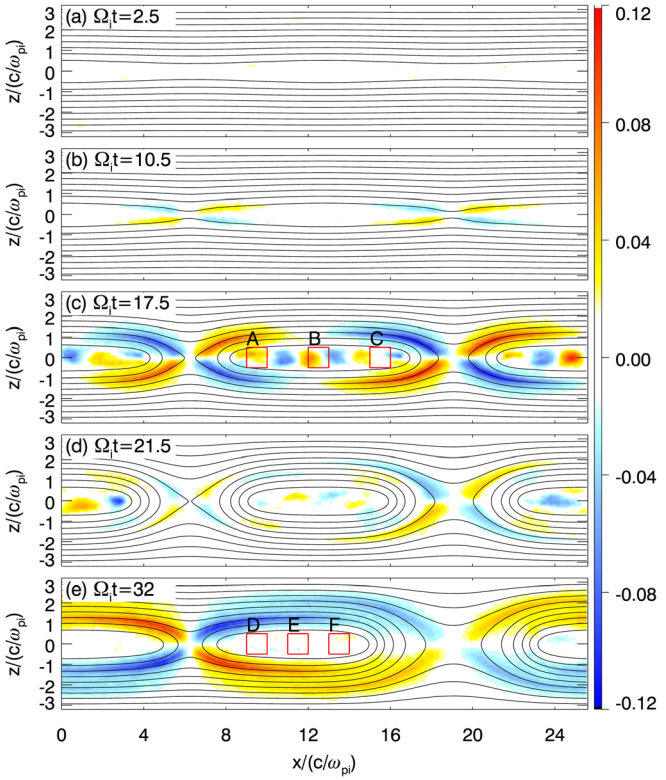

FIG. 1. (Color online) The time evolution of the out-of-plane magnetic field B_y/B_0 during collisionless magnetic reconnection at $\Omega_i t$ =2.5, 10.5, 17.5, 21.5, and 32 for Run 1, and the corresponding magnetic field lines are also plotted in the figure.

of B_y with the quadrupole structures around the X-lines increases, and at the same time regular structures of B_y with alternative values along the x direction are formed in the magnetic islands. At $\Omega_i t$ =17.5 as shown in Fig. 1(c), the maximum amplitude of B_y around the X-lines is about $B_y/B_0 \sim 0.1$, while it is about $B_y/B_0 \sim 0.06$ inside the magnetic islands. The scale length between the positive and negative values of B_y is about 2.4 c/ω_{pi}. With the saturation of the reconnection, the amplitude of B_y both around the X-lines and inside the magnetic islands decreases. The structures of B_y disappear at about $\Omega_i t$ =28.

Figure 2 shows the electron velocity distributions inside the magnetic island at $\Omega_i t$ =17.5 for Run 1. The top panel shows the electron distributions in the phase space (v_x, v_z), and the bottom panel depicts the distributions in the phase space (v_x, v_y). The labels A, B, and C denote the regions (marked in Fig. 1(c)) where the distributions are calculated. The electron distributions are anisotropic, and there are no obvious flows in the magnetic island. The temperature in the x direction is larger than that in the y and z directions. The anisotropy of electron distributions can be demonstrated more clearly in Fig. 3, which depicts the electron temperatures $T_{||e}/T_{||e0}$, $T_{\perp e}/T_{\perp e0}$, and the anisotropy $A_e = T_{||e}/T_{\perp e} - 1$ at $\Omega_i t$ =17.5 for Run 1. The parallel temperature is much larger than the perpendicular temperature in the magnetic islands. Such anisotropic distributions are the results of the moving electrons along the magnetic field lines after they are accelerated by the reconnection electric field.

Figure 4 shows the electron velocity distributions inside the magnetic island at $\Omega_i t$ =32 for Run 1. The top panel

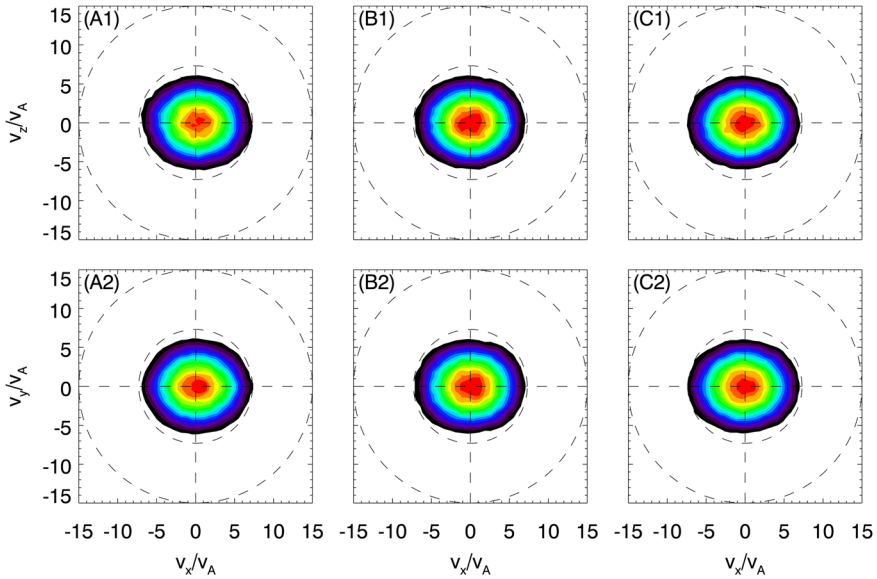

FIG. 2. (Color online) The electron velocity distributions $f(v_x, v_z)$ (the top panel) and $f(v_x, v_y)$ at the time $\Omega_i t = 17.5$, in three different regions: (A) $x \in [9, 10]c/\omega_{pi}$, $z \in [-0.5, 0.5]c/\omega_{pi}$; (B) $x \in [12, 13]c/\omega_{pi}$, $z \in [-0.5, 0.5]c/\omega_{pi}$; and (C) $x \in [15, 16]c/\omega_{pi}$, $z \in [-0.5, 0.5]c/\omega_{pi}$. The regions are marked by A, B, and C in Fig. 1, and the dashed lines denote the bound of a symmetric distribution.

shows the electron distributions in the phase space (v_x, v_z) and the bottom panel depicts the distributions in the phase space (v_x, v_y). The labels D, E, and F denote the regions (marked in Fig. 1(e)) where the distributions are calculated. Figure 5 plots the electron temperatures $T_{||e}/T_{||e0}$, $T_{\perp e}/T_{\perp e0}$, and the anisotropy $A_e = T_{||e}/T_{\perp e} - 1$ at $\Omega_i t = 32$ for Run 1. Now the electron distributions in the magnetic islands are almost isotropic, and the regular structures of the out-of-plane magnetic field cannot be found. Therefore, such structures are related to the temperature anisotropy. This can be confirmed in Fig. 6, which shows the out-of-plane magnetic field B_y/B_0 at $\Omega_i t$ =2.5, 10.5, and 17.5 for Run 1, and the magnetic field lines in the (x, z) plane are also plotted in the figure. However, now at $\Omega_i t = 16$, just before the regular structures of B_y are formed inside the magnetic islands we introduce a pitch angle scattering operator in the particle push, as done before by Karimabadi *et al.*[26] The scattering tries to make the electron distribution isotropic and the temperature anisotropy is removed, while the electron average velocity and kinetic energy are kept as before. Unlike in Fig. 1, at $\Omega_i t = 17.5$ we cannot find that the regular structures of B_y are formed inside the magnetic islands. This confirms that the regular structures are related to the electron temperature anisotropy.

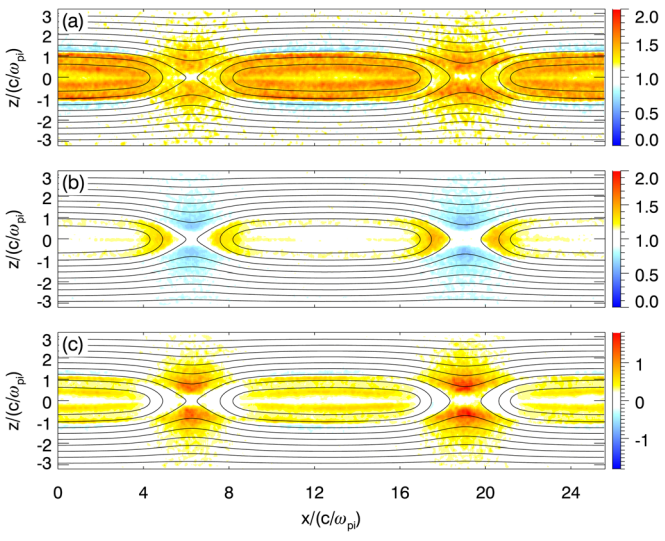

FIG. 3. (Color online) The electron temperatures (a) $T_{||e}/T_{||e0}$, (b) $T_{\perp e}/T_{\perp e0}$, and (c) the anisotropy $A_e = T_{||e}/T_{\perp e} - 1$ at $\Omega_i t$ =17.5 for Run 1.

In the magnetic islands the plasma is anisotropic and the magnetic field is very weak, therefore it is unstable to the Weibel instability.[27] The regular structures of B_y inside the magnetic islands are considered to be the results of the Weibel instability. However, according to the linear theory in homogeneous plasma, the waves excited by the Weibel instability should have wave vector along the z direction. In the follows, we will demonstrate that regular structures similar to that in Fig. 1 can be formed due to the Weibel instability in a current sheet with a small width, which is comparable to the wavelength of the Weibel instability predicted by the linear theory.

Figure 7 shows the time evolution of the out-of-plane magnetic field B_y/B_0 at $\Omega_i t$ =1, 2, 3, and 7 for Run 2. The Weibel instability can be excited in the center of the current sheet. At first the wave vector of the excited waves is almost along the z direction due to the temperature anisotropy, and the wavelength is about 1.1 c/ω_{pi} when $A_{e0} = T_{||e0}/T_{\perp e0} - 1 = 0.8$. Linear analysis found that the growth rate is maximum at $k_z^2 = \frac{1}{3} A_e \frac{\omega_{pe}^2}{c^2}$, and the corresponding wavelength is about $1.2c/\omega_{pi}$ in a homogeneous plasma.[28] Our simulation results are consistent with the linear theory in Run 2. At last, it forms the structures with alternate positive and negative values of the out-of-plane magnetic field along the x direction as observed in the magnetic islands (see Fig. 1). However, when the wavelength of the excited Webel instability is comparable to the width of the current sheet, the structures with alternate positive and negative values of the out-of-plane magnetic field along the x direction will be formed. This is shown in Fig. 8, which plots the time evolution of the out-of-plane magnetic

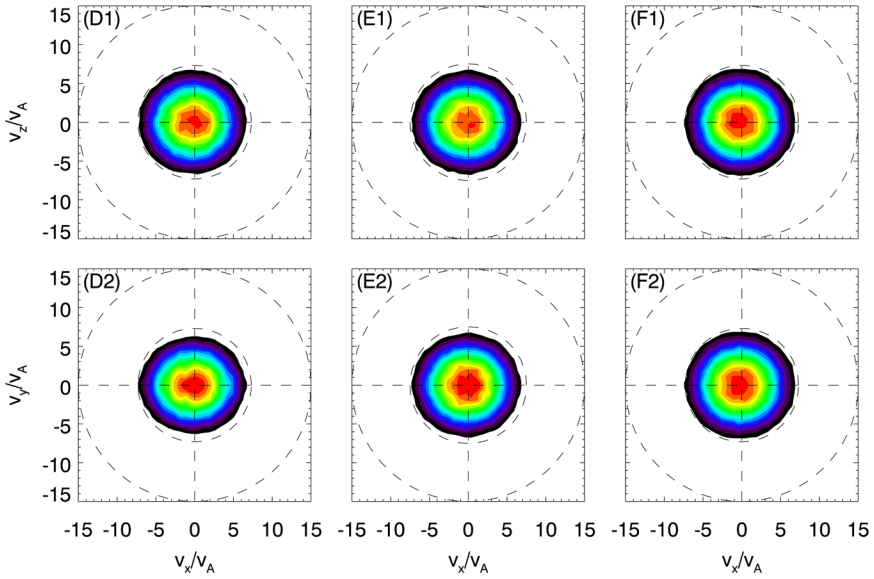

FIG. 4. (Color online) The electron velocity distributions $f(v_x, v_z)$ (the top panel) and $f(v_x, v_y)$ at the time $\Omega_i t = 32$, in three different regions: (A) $x \in [9, 10]c/\omega_{pi}$, $z \in [-0.5, 0.5]c/\omega_{pi}$; (B) $x \in [12, 13]c/\omega_{pi}$, $z \in [-0.5, 0.5]c/\omega_{pi}$; and (C) $x \in [15, 16]c/\omega_{pi}$, $z \in [-0.5, 0.5]c/\omega_{pi}$. The regions are marked by D, E, and F in Fig. 1, and the dashed lines denote the bound of a symmetric distribution.

field B_y/B_0 at $\Omega_i t = 1$, 2, 3, and 7 for Run 3. In summary, when the wavelength of the excited Weibel instability by the electron temperature anisotropy is comparable to the width of the current sheet, the structures with alternate positive and negative values of the out-of-plane magnetic field along the x direction will be formed.

IV. CONCLUSIONS AND DISCUSSION

The Weibel instability has been investigated inside the electron-positron Harris sheet, where structures of the out-of-plane magnetic field are fromed.[29,30] Baumjohann *et al.*[31] studied the structures of the out-of-plane magnetic field inside the electron inertial region in the electron-proton current sheet. They found that the inflow of electrons into the sheet from its two sides may well be capable of self-consistently generating a weak magnetic guide field via the Weibel instability. In this paper, 2D PIC simulations are employed to investigate the structures of magnetic island formed during anti-parallel reconnection. Alternate positive and negative values of the out-of-plane magnetic field along the x direction are observed in magnetic island for the first time. Such structures are considered to be the results of the Weibel instability in magnetic island, which is driven by the electron temperature anisotropy. The electron temperature anisotropy is the result of accelerated electrons by the reconnection electric field. The existence of the out-of-plane magnetic field inside magnetic island may affect the process of electron acceleration in magnetic island, which is our further investigation. We also perform the cases with an initial guide field, and find that such structures will disappear even if a small guide field ($\sim 0.1B_0$) is added. Therefore, these structures are sensitive to a guide field.

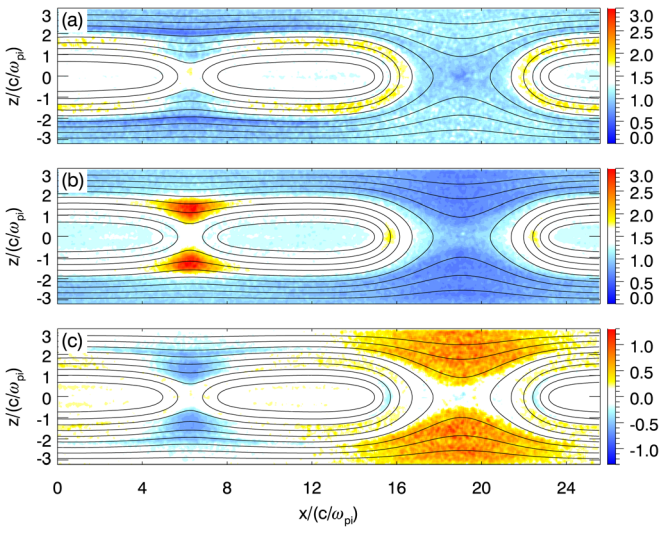

FIG. 5. (Color online) The electron temperatures (a) $T_{||e}/T_{||e0}$, (b) $T_{\perp e}/T_{\perp e0}$, and (c) the anisotropy $A_e = T_{||e}/T_{\perp e} - 1$ at $\Omega_i t = 32$ for Run 1.

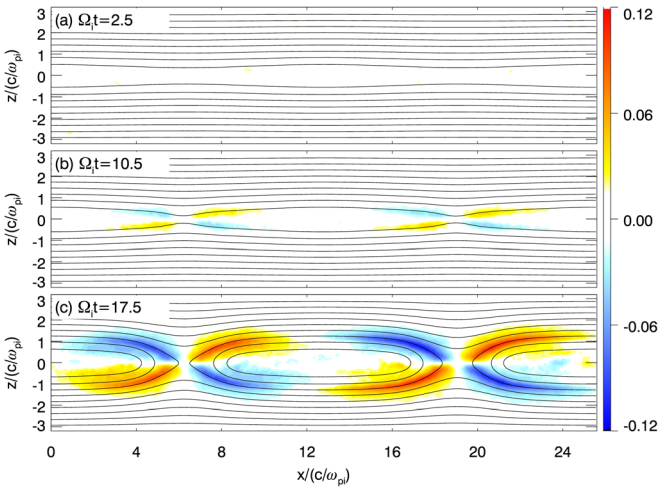

FIG. 6. (Color online) The time evolution of the out-of-plane magnetic field B_y/B_0 during collisionless magnetic reconnection at $\Omega_i t = 2.5$, 10.5, and 17.5 for Run 1, and the corresponding magnetic field lines are also plotted in the figure. Different from in Fig. 1, now at $\Omega_i t = 16$, just before the regular structures of B_y inside the magnetic islands are formed, a pitch angle scattering operator is introduced in the particle push to make the electron distribution isotropic.

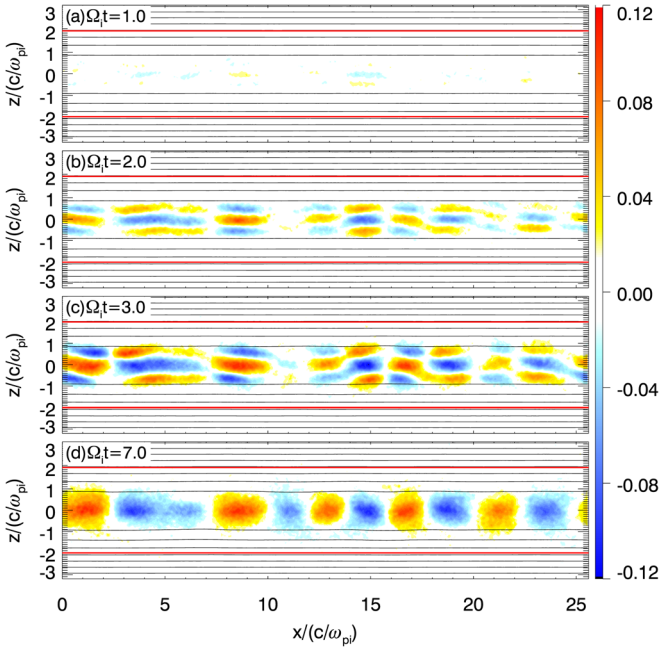

FIG. 7. (Color online) The time evolution of the out-of-plane magnetic field B_y/B_0 at $\Omega_i t$ =1, 2, 3, and 7 for Run 2. The width of the corresponding Harris current sheet is also marked with thick solid lines.

One thing we should note is that in magnetic island the direction of the wave vector k of the Weibel instability in the PIC simulations is different from that in the linear expectation, which is parallel to the direction of minimum temperature. The nonlinear effects, which arise when the width of the current sheet is comparable to the wavelength predicted by the linear theory, are considered to cause this difference. However, how the nonlinear effects will influence the Weibel instability needs further investigation.

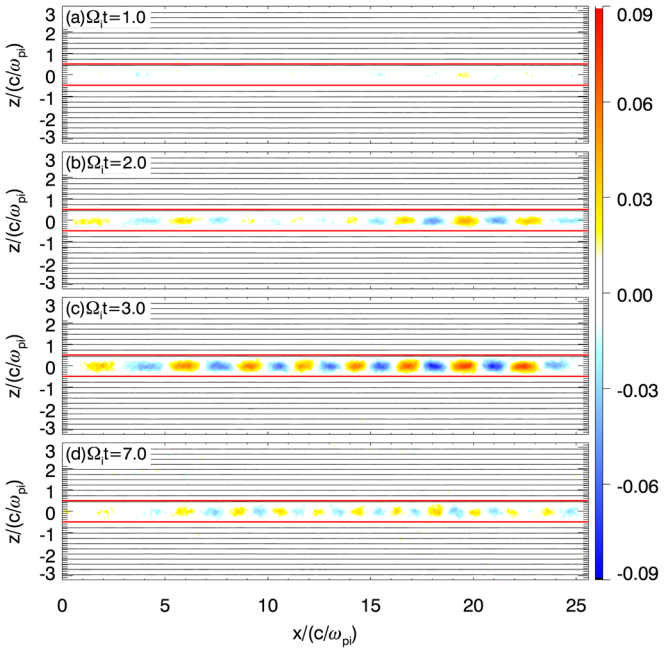

FIG. 8. (Color online) The time evolution of the out-of-plane magnetic field B_y/B_0 at Ω_i t =1, 2, 3, and 7 for Run 3. The width of the corresponding Harris current sheet is also marked with thick solid lines.

ACKNOWLEDGMENT

This research was supported by the National Science Foundation of China, Grant Nos. 40931053, 40725013, and 40974081, the Specialized Research Fund for State Key Laboratories, and the Fundamental Research Funds for the Central Universities (WK2080000010). PHY acknowledges support by the Korean Ministry of Education, Science and Technology, under WCU Grant No. R31-10016.

[1]V. M. Vasyliunas, Rev. Geophys. **13**, 303, doi: 10.1029/RG013i001p00303 (1975).
[2]D. Biskamp, *Magnetic Reconnection in Plasmas* (Cambridge University Press, Cambridge, 2000).
[3]E. R. Priest and T. Forbes, *Magnetic Reconnection: MHD Theory and Applications* (Cambridge University Press, New York, 2000).
[4]P. L. Pritchett, J. Geophys. Res. **111**, A10212, doi:10.1029/2006JA011793 (2006).
[5]M. Hoshino, T. Mukai, T. Terasawa, and I. Shinohara, J. Geophys. Res. **106**, 25979, doi: 10.1029/2001JA900052 (2001).
[6]X. R. Fu, Q. M. Lu, and S. Wang, Phys. Plasmas **13**, 012309 (2006).
[7]J. F. Drake, M. A. Shay, and W. Thongthai, Phys. Rev. Lett. **94**, 095001 (2005).
[8]R. P. Lin and H. S. Hudson, Sol. Phys. **17**, 412 (1971).
[9]R. P. Lin and H. S. Hudson, Sol. Phys. **50**, 153 (1976).
[10]J. A. Miller, P. J. Cargill, A. Emslie, G. D. Holamn, B. R. Dennis, T. N. Larosa, R. M. Winglee, S. G. Benka, and S. Tsuneta, J. Geophys. Res. **102**, 14631, doi: 10.1029/97JA00976 (1997).
[11]M. Øieroset, R. P. Lin, T. D. Phan, D. E. Larson, and S. D. Bale, Phys. Rev. Lett. **89**, 195001 (2002).
[12]S. Imada, R. Nakamura, P. W. Daly, M. Hoshino, W. Baumjohann, S. Mühlbachler, A. Balogh, and H. Rème, J. Geophys. Res. **112**, A03202, doi: 10.1029/2006JA011847 (2007).
[13]L. J. Chen, A. Bhattacharjee, P. A. Puhl-Quinn, H. Yang, N. Bessho, S. Imada, S. Mühlbachler, P. W. Daly, B. Lefebvre, Y. Khotyaintsev, A. Vaivads, A. Fazakerley, and E. Georgescu, Nat. Phys. **4**, 19 (2008).
[14]R. S. Wang, Q. M. Lu, C. Huang, and S. Wang, J. Geophys. Res. **115**, A01209, doi: 10.1029/2009JA014553 (2010).
[15]R. S. Wang, Q. M. Lu, A. M. Du, and S. Wang, Phys. Rev. Lett. **104**, 175003 (2010).
[16]R. S. Wang, Q. M. Lu, X. Li, C. Huang, and S. Wang, J. Geophys. Res. **115**, A11201, doi: 10.1029/2010JA015473 (2010).
[17] P. L. Pritchett, J. Geophys. Res. **106**, 3798, doi: 10.1029/2001JA000016 (2001).
[18]P. L. Pritchett and F. V. Coroniti, J. Geophys. Res. **109**, A01220, doi: 10.1029/2003JA009999 (2004).
[19]Q. M. Lu, C. Huang, J. L. Xie, R. S. Wang, M. Y. Wu, A. Vaivads, and S. Wang, J. Geophys. Res. **115**, A11208, doi: 10.1029/2010JA015713 (2010).
[20]C. Huang, Q. M. Lu, and S. Wang, Phys. Plasmas **17**, 072306 (2010).
[21]L. J. Chen, N. Bessho, B. Lefebvre, H. Vaith, A. Asnes, O. Santolik, A. Fazakerley, P. Puhl-Quinn, A. Bhattacharjee, Y. Khotyaintsev, P. Daly, and R. Torbert, Phys. Plasmas **16**, 056501 (2009).
[22]M. Oka, M. Fujimoto, I. Shinohara, and T. D. Phan, J. Geophys. Res. **115**, A08223, doi: 10.1029/2010JA015392 (2010)
[23]K. G. Tanaka, T. Yumura, M. Fujimoto, I. Shinohara, S. V. Badman, and A. Grocott, Phys. Plasmas **17**, 102902 (2010).
[24]K. B. Quest, H. Karimabadi, and W. Daughton, Phys. Plasmas **17**, 022107 (2010).
[25]H. Karimabadi, W. Daughton, and K. B. Quest, Geophys. Res. Lett. **31**, L18801, doi: 10.1029/2004GL020791 (2004).
[26]H. Karimabadi, W. Daughton, and K. B. Quest, J. Geophys. Res. 110, A03214, doi: 10.1029/2004JA010749 (2005).
[27]E. S. Weibel, Phys. Rev. Lett. **2**, 83 (1959).
[28]N. A. Krall and A. W. Trivelpiece, *Principle of Plasma Physics* (McGraw-Hill, New York, 1973).
[29]S. Zenitani and M. Hesse, Phys. Plasmas **15**, 022101 (2008).
[30]Y. H. Liu, M. Swisdak, and J. F. Drake, Phys. Plasmas **16**, 042101 (2009).
[31]W. Baumjohann, R. Nakamura, and R. A. Treumann, Ann. Geophys. **28**, 789, (2010).